



Fermi National Accelerator Laboratory

TM-1450
(SSC-N-320)
0102.001

Full Length Prototype SSC Dipole Test Results*

J. Strait, B.C. Brown, J. Carson, N. Engler, H.E. Fisk, R. Hanft, K. Koepke,
M. Kuchner, E. Larson, R. Lundy, P. Mantsch, P.O. Mazur, A. McInturff,
T. Nicol, T. Ohmori, E.E. Schmidt, J. Theilacker, and G. Tool
Fermi National Accelerator Laboratory,
P.O. Box 500, Batavia, Illinois 60510

J. Cottingham, P. Dahl, M. Garber, A. Ghosh, C. Goodzeit, A. Greene,
J. Herrera, S. Kahn, E. Kelly, G. Morgan, A. Prodell, W. Sampson,
W. Schneider, R. Shutt, P. Thompson, P. Wanderer, and E. Willen
Brookhaven National Laboratory
Upton, New York 11973

S. Caspi, W. Gilbert, W. Hassenzahl, R. Meuser, C. Peters, J. Rechen, R. Royer,
R. Scanlan, and C. Taylor
Lawrence Berkeley Laboratory
University of California
Berkeley, California 94720

April 24, 1987

*Presented at the 1986 Applied Superconductivity Conference, Baltimore, MD, September 28 - October 3, 1987.



FULL LENGTH PROTOTYPE SSC DIPOLE TEST RESULTS*

J. Strait, B. C. Brown, J. Carson, N. Engler, H. E. Fisk, R. Hafft, K. Koepke, M. Kuchnir, E. Larson, R. Lundy, P. Mantsch, P. O. Mazur, A. McInturff, T. Nicol, T. Omori,[†] E. E. Schmidt, J. Theilacker, and G. Tool
Fermi National Accelerator Laboratory
P. O. Box 500
Batavia, Illinois 60510

J. Cottingham, P. Dahl, M. Garber, A. Ghosh, C. Goodzeit, A. Greene, J. Herrera, S. Kahn, E. Kelly, G. Morgan, A. Prodell, W. Sampson, W. Schneider, R. Shutt, P. Thompson, P. Wanderer, and E. Willen
Brookhaven National Laboratory
Upton, New York 11973

S. Caspi, W. Gilbert, W. Hassenzuhl, R. Meuser, C. Peters, J. Rechen, R. Royer, R. Scanlan, and C. Taylor
Lawrence Berkeley Laboratory
University of California
Berkeley, California 94720

Abstract

Results are presented from tests of the first full length prototype SSC dipole magnet. The cryogenic behavior of the magnet during a slow cooldown to 4.5K and a slow warmup to room temperature has been measured. Magnetic field quality was measured at currents up to 2000 A. Averaged over the body field all harmonics with the exception of b_2 and b_4 are at or within the tolerances specified by the SSC Central Design Group. (The values of b_2 and b_4 result from known design and construction defects which will be corrected in later magnets.) Using an NMR probe the average body field strength is measured to be 10.283 G/A with point to point variations on the order of one part in 1000. Data are presented on quench behavior of the magnet up to 3500 A (approximately 55% of full field) including longitudinal and transverse velocities for the first 250 msec of the quench.

Introduction

In this paper we present test results from the first full scale prototype magnet¹ for the proposed Superconducting Super Collider (SSC).² A cross section of this magnet (designated design D) is shown in Fig. 1. The magnet has a "cos θ " style coil with a 4 cm aperture and a magnetic length of 16.6 m. The operating field is 6.6 T at a current of 6400 A. The coil is collared with stainless steel laminations and surrounded by a cylindrical iron yoke with an inner diameter of 11 cm and an outer diameter of 27 cm. Inside the main coil is a superconducting sextupole trim coil wound on the beam pipe. This coil compensates for distortions of the dipole field due to persistent current effects at low field and to iron saturation at high field. The coil is cooled primarily by heat conduction through the collar and yoke laminations to 4.5K, 4 atm helium flowing in four coolant channels in the iron. Approximately 1% of the flow passes through the 1.4 mm annular space between the trim and main coils to provide good heat conduction from the beam pipe and the coil to the collars.

The cryostat³ includes aluminum heat shields operating at 20K and 80K inside a 60 cm diameter vacuum vessel made of mild steel. The cold mass is supported by five re-entrant posts made of fiberglass

* Work supported by the U.S. Department of Energy.

[†] Permanent address Ishikawajima-Harima Heavy Industries Co., Yokohama, Japan.

Manuscript received September 30, 1986.

reinforced plastic (FRP) tubes with metallic junctions. The magnet is free to slide longitudinally on four of the five posts to allow for thermal contraction, while axial restraint is provided at the center post by two FRP anchors which run at an approximately 30 degree angle between the base of the post and the cold mass. The cold mass of one magnet is connected to the next by a bellows assembly with a diameter equal to the cold mass, yielding a reservoir of 40 liters of helium between magnets.

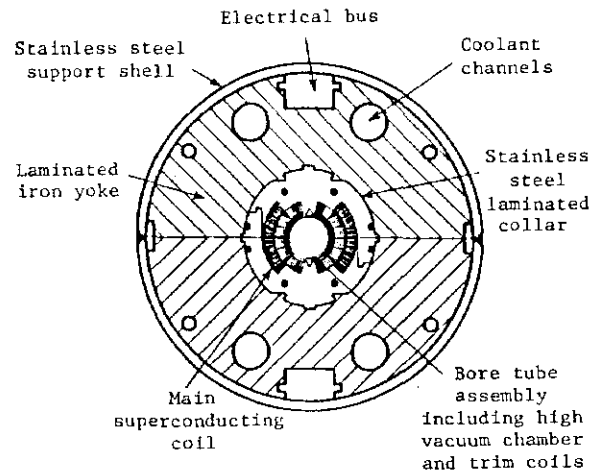


Figure 1. SSC dipole magnet cold mass cross section.

Test Facility

The tests reported here were carried out at the Fermilab Magnet Development and Test Facility. This facility has been previously used for production testing of superconducting magnets for the Tevatron; one Tevatron test stand was replaced for these tests. Liquid helium is provided by a CTI-1500 refrigerator,⁴ while electrical power for the magnet is supplied by two Transrex power supplies.

Refrigeration

Cryogens from the refrigerator and electric power and instrumentation lines are routed to the magnet under test through a "feed can" whose end simulates a neighboring magnet. Four atmosphere, 4.5K helium flows through the magnet cold mass and at the "turnaround can" is directed back through the liquid return line in the magnet cryostat. In the feed can, part of the returned helium passes through a J-T valve into the snell side of a heat exchanger to cool the

incoming helium. The outflow from the heat exchanger is recombined with the remainder of the helium and is directed through the magnet gas return line. At the turnaround the helium is returned to the feed can through the 20K shield. This mode of operation puts the 20K shield at approximately 4.7K. The 80K shield is cooled by liquid nitrogen which is vented to atmosphere after a single pass through the magnet.

Cryogenic Instrumentation

The temperature of the helium in the interconnect regions at each end of the magnet is monitored with carbon-glass⁵ and germanium⁶ resistance thermometers and with vapor pressure thermometers. The coil on this first prototype magnet is wound with flared ends ("dogbones"),⁷ allowing the placement of 100 Ω , 1/8 W carbon resistors inside the ends of the coil. These resistors measure the temperature of the helium exiting the coil before it is mixed with the much larger flow through the coolant channels in the iron yoke. Helium pressure is measured at both ends of the magnet with strain gage pressure transducers⁸ which are connected to the magnet by capillary tubes. Pressure in the coolant channels at the center of the magnet is measured with a piezoelectric pressure transducer⁹ operated at liquid helium temperature. Helium flow is monitored by measuring the differential pressure across a venturi located in the feed can. Half bridge strain gages are mounted on the axial restraint anchors to measure forces on the magnet. To monitor the loading of the coil, full bridge strain gages are mounted on aluminum blocks that are placed between the collars and the coil about 30 cm into the magnet.

Data from these and other transducers are collected every 10 minutes by a VAX 11/730 computer through a relay scanner¹⁰ and digital multimeter.¹¹ The measurements are converted to physical units, displayed for the refrigerator operators and recorded on disk for later analysis. Temperatures in the interconnect regions and in the dogbone ends of the coil, pressures in the interconnect regions and at the magnet center, and the strains on the center anchors are also recorded by a fast ADC¹² during and immediately after a quench.

Electrical Instrumentation

The main coil is wound in four parts: lower inner, lower outer, upper outer and upper inner coils. For quench detection and analysis, taps on the magnet allow the monitoring of voltages separately across each quarter coil. In addition voltage taps are placed across the superconducting part of the power leads from the feed can to the magnet and across the trim coil. Current is measured with a 10 $\mu\Omega$ shunt¹³ and dI/dt is measured with an air core mutual inductor (dI/dt coil) allowing the extraction of the resistive component of the magnet voltage.

Quenches are detected by four safety circuits whose thresholds are shown in Table 1. Quench protection is provided by an external 0.2 Ω dump resistor and by strip heaters which run the full length of the magnet between the outer coil and the collars at four azimuthal positions. Normally, two strip heaters in opposite quadrants are used. The triggering of the dump and of the protection heaters may be independently delayed to allow study of "natural" quench development. Relief valves, normally set to open at 85 psia, are opened electronically (with an optional delay) when a quench is detected. Test quenches may be induced by any of four "spot" heaters located along the parting plane between the

upper and lower inner coils approximately 60 cm into the coil (beyond the dogbone ends) from each end.

Voltages across each main coil quarter, the trim coil, the power leads, the dI/dt coil, the shunt, the external dump and the strip and spot heaters are digitized during a quench by a fast ADC¹² and recorded on disk by a VAX 11/730 computer. An on-line analysis program checks the data for internal consistency, computes maximum total and resistive voltages for each quarter coil and computes the time integral of I^2 (MIITs) from the time the quench is detected. On-line displays are provided of all electrical and cryogenic quantities recorded during a quench.

Table 1

Quench detection safety circuit thresholds

Lower half coil - Upper half coil	0.25	Volts
Magnet total voltage	6.5	Volts
Magnet voltage - L (dI/dt)	8.0	Volts ¹⁴
Positive - Negative power lead	0.025	Volts
Trim coil voltage	0.5	Volts
Ground Fault Current	3.0	A

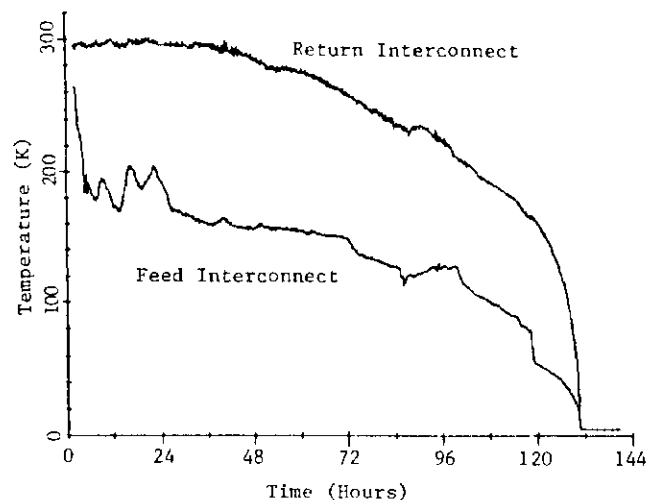


Figure 2. Temperature in the feed and return interconnect regions as a function of time during the cooldown of the SSC magnet.

Magnet Cooldown Data

The magnet was cooled to 4.5K over a period of five days. To reduce the effect of differential thermal contractions the temperature difference between the two ends of the magnet was limited to about 100K. The temperature of the helium supplied to the magnet was controlled by mixing cold helium from the refrigerator with room temperature helium. Temperature was further moderated by maintaining the shell side of the heat exchanger in the feed can at the temperature of the magnet outlet gas. Fig. 2 shows the temperature at the two ends of the magnet as a function of time during the cooldown. The measured strain on the two center anchors is plotted in Fig. 3. A change of approximately -2000 micro-strain is predicted from room temperature to 4.5K due to differences in thermal contraction among the anchor, the center post and the magnet. The larger measured change and the rapid change as the magnet approaches liquid helium temperature probably reflect the lack of

perfect temperature compensation in the half bridges. A number of abrupt changes in strain can be seen. These occur when the slide mechanism on one of the outer four posts sticks and then breaks loose. The largest such step (140 micro-strain) corresponds to 20-25% of the breaking strength of a post.¹⁵

Stress-strain relations for the aluminum blocks that measure the coil loading were calibrated both at room temperature and at 4.5K before the blocks were mounted in the coil. At the beginning of the cooldown the coil pre-stress was measured to be 3000 psi for the inner coil and 3500 psi for the outer coil. The pre-stress loss in cooling to liquid helium temperature was 1400 psi in both coils. Upon warming the magnet to room temperature after about a month of testing, both coils returned to their original pre-stress.

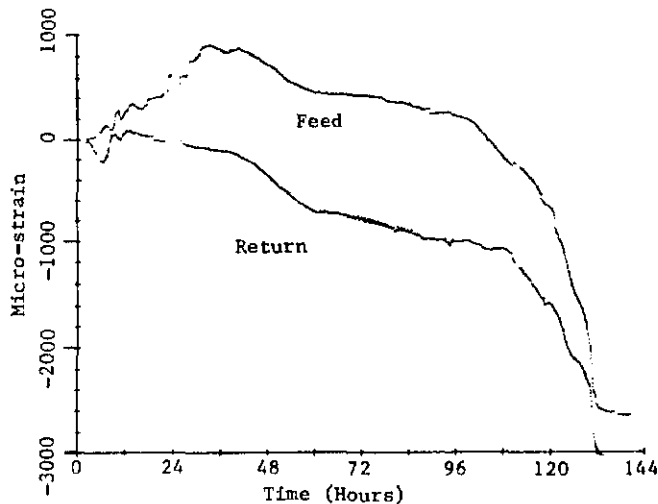


Figure 3. Strain on the two axial restraint anchors during cooldown of the SSC magnet.

Magnetic Measurements

The magnetic field quality was measured at currents up to 2000 A before attempting to bring the magnet to full field. The field strength was measured with an NMR probe¹⁶ while the harmonic content was measured with a rotating coil probe called the "mole."¹⁷ Because the beam pipe in this magnet is in contact with the 4.5K helium, a "warm bore" tube must be inserted inside the cold bore in order to allow the use of room temperature probes. The warm bore consists of a Nitronic 40 stainless steel tube with an outside diameter of 29.6 mm and a wall thickness of 0.38 mm which is wrapped with 20 layers of superinsulation. The 1.6 mm annular space between the warm and cold bores is evacuated. The warm bore is centered by small cones of glass bead filled epoxy attached to the warm bore tube at 1 meter intervals.

Field Strength Measurements

The absolute field strength was measured using an NMR probe designed to fit into the small diameter warm bore. The probe is similar to those used to measure Tevatron magnets¹⁸ but with a number of differences. The sensitive material is a gum rubber cylinder 5 mm in diameter by 15 mm long. The short dimension of the sample volume is along the bore tube direction allowing very small structures to be observed. The package includes a Hall probe which extends the dynamic range, allows easier tuning of the NMR

frequency and enables the mapping of the end regions of the magnet. An internal dipole coil may be powered to align the sample perpendicular to the magnetic field, maximizing the signal to noise ratio. The NMR frequency is converted to gauss in hardware and the field strength and current are read by a VAX 11/730. The probe is moved manually through the magnet and position is read from a fiberglass measuring tape. The uncertainty in position is estimated to be less than 3 mm.

The transfer function (field strength divided by magnet current) was measured at 1900 A in 2.54 cm intervals. The results are shown in Fig. 4. To check accuracy and repeatability, almost half the magnet was scanned a second time in 7.62 cm intervals and a 30.48 cm region around one particularly narrow dip was measured a third time in 1.27 cm intervals. Comparisons of the three scans measures not only the stability of the electronics but also the repeatability of the positioning. In addition 35 measurements were taken over a period of 13 minutes at a fixed position and current. From these data, the rms repeatability is estimated to be 25 ppm. Thus, almost all of the structure observed in Fig. 4 is real and rapid changes in transfer function over distances of a few centimeters are easily observed. The most striking features are the large dips which occur every 152 cm. This length corresponds to a periodicity in the press used during the curing of the epoxy impregnated coils which presumably causes small variations in coil dimensions. The absolute accuracy of the transfer function measurement is dominated by the uncertainty of approximately 5×10^{-4} in the calibration of the shunt used to measure the current.

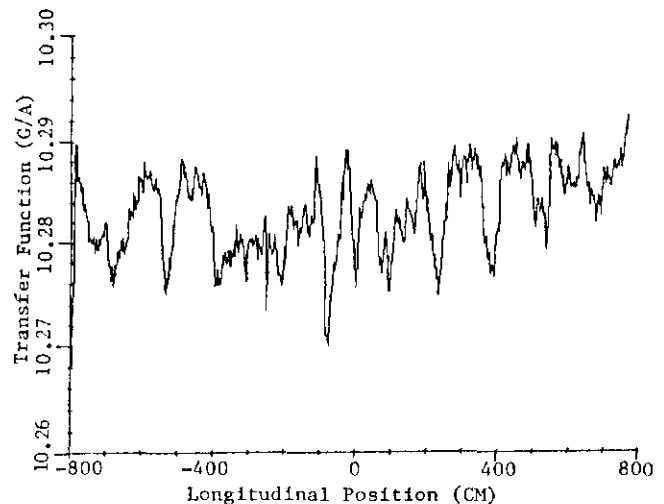


Figure 4. Transfer function (magnetic field strength divided by magnet current) versus position as measured with an NMR probe. The origin is at the center of the magnet and positive positions are towards the lead end.

Harmonic Multipole Measurements

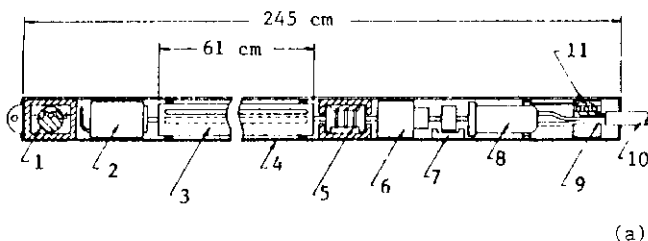
The field shape of accelerator magnets is generally expressed in terms of a two dimensional multipole expansion:

$$B_y + iB_x = B_0 \sum_{n=0}^{\infty} (b_n + ia_n) \left((x + iy)/r_{ref} \right)^n$$

where r_{ref} is the reference radius; r_{ref} is chosen to be 1 cm for SSC magnets. In the notation used here,

the harmonics allowed by the symmetry of the coil are b_n with n even. The allowed harmonics, particularly those of lower order, are expected to have larger systematic values than the other harmonics and to display persistent current hysteresis effects.

The mole (see Fig. 5) measures the harmonic content of the magnetic field using a 61 cm long, 2.40 cm diameter rotating coil. The coil is turned by an air motor at a speed of one revolution per 3.5 seconds. The probe carries three coils. A small opening angle tangential coil measures the radial component of the field, while two bucking coils allow the dominant dipole term to be subtracted from the measuring coil signal. This allows the extraction of higher harmonics with a sensitivity of a few parts per million of the dipole field. The mole assembly also includes a gravity sensor which is coupled to the encoder that reads coil angle, allowing the dipole field angle to be measured. The coil signals are brought out via slip rings and are measured by three digital voltmeters.¹¹ A mini-computer¹⁹ collects the data and extracts the harmonic coefficients. The mole has been calibrated at 2 T in a large aperture, harmonic free iron dipole magnet and at 4 T in a harmonic rich Tevatron magnet. The probe is capable of measuring field angle to several tenths of a milliradian and harmonics to better than 0.1 unit at 1 cm.



- | | |
|-----------------------------|--------------------------|
| 1. Gravity Sensor | 6. Reducer |
| 2. Precision Encoder | 7. Speed Indicator |
| 3. Tangential Coil Assembly | 8. Gas Motor |
| 4. Outer Skin | 9. Gas Inlet and Exhaust |
| 5. Slip Rings | 10. Tether |
| | 11. Junction Box |

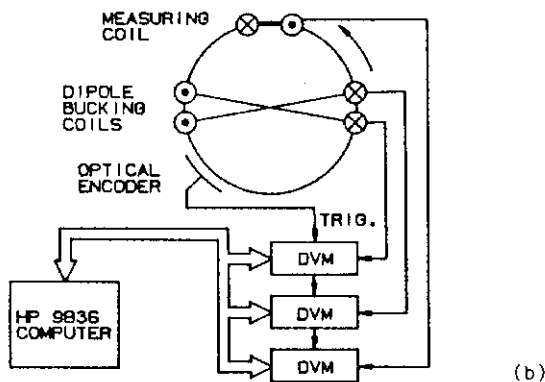


Figure 5. The mole. (a) Longitudinal cross section showing drive mechanism and coil location. (b) Schematic transverse cross section showing coil azimuthal locations and readout system.

Since there will be approximately 8000 dipoles in the SSC, it is desirable not to test cryogenically each magnet before installation in the ring. One of the important tests in the prototyping stage is to verify that a measurement of the harmonics and field angle at low current, with the magnet warm and with

the remnant field in the iron not yet set, will adequately predict the behavior of the magnet at high field. Therefore the mole was used to measure the field quality at 10 A before the magnet was cooled and at 2000 A with the magnet at 4.5K. The magnet is approximately 17 meters long while the measuring coil is 0.61 meters, requiring the field to be measured at 28 positions to cover the full length. The central 26 points are in the body field region and the two outer positions characterize the end fields.

The results, averaged over the 26 body field positions, are compared in Table 2. The data have been corrected for off-centering of the probe independently at each position by assuming that any non-zero value of the 16-pole term results from feed-down from the 18-pole. Also shown for comparison are the specifications²⁰ given by the SSC Central Design Group. With the exception of a_1 and b_2 , warm and cold measurements agree within one or two tenths of a unit. The warm value of b_2 is 0.7 units larger than the cold value because, with the large filaments in the cable used in this magnet (20 micron compared with 5 microns in the final design), there is still a non-zero persistent current contribution to the sextupole moment at 2000 A. In fact, hysteresis is observed in all the allowed multipoles (b_n with n even) and the warm-cold agreement is, in general, not as good for these as for the disallowed harmonics. The disagreement in a_1 is not understood. All harmonics except b_2 and b_8 are at or within the specifications. The large values of these two coefficients result from known defects in the coil design and construction which will be corrected in later magnets. Point-to-point variations in harmonic coefficients have also been investigated and reasonable uniformity has been found. Fig. 6 displays, for example, the values of the normal (b_1) and skew (a_1) quadrupole moments versus position.

Table 2

Harmonic multipole coefficients measured at 10 A with the magnet at room temperature ("warm") and at 2000 A with the magnet at 4.5K ("cold"), compared with specifications for random and systematic components. Units for a_n and b_n are 10^{-4} cm⁻ⁿ.

	Warm	Cold	Random	Systematic
a_1	0.8	-0.8	0.7	0.2
a_2	-0.3	-0.3	0.6	0.1
a_3	0.0	-0.1	0.7	0.2
a_4	0.0	-0.1	0.2	0.2
a_5	0.0	-0.1	0.2	---
a_6	0.0	0.0	0.1	---
a_7	0.0	0.0	0.2	---
a_8	0.0	0.0	0.1	---
b_1	0.1	0.1	0.7	0.2
b_2	-11.8	-12.5	2.0	0.1
b_3	0.0	0.0	0.3	0.1
b_4	0.1	0.4	0.7	0.2
b_5	0.0	0.0	0.1	0.02
b_6	0.2	0.1	0.2	0.04
b_7	0.0	0.0	0.2	0.06
b_8	0.8	0.8	0.1	0.1
B_0/I	10.33	10.25 G/A		
A_0/B_0	4.1	2.7 mrad		

Quench Behavior

After magnetic measurements were completed, the quench behavior of the magnet was studied. Since this

was the first time a magnet of this design was powered, a cautious approach to bringing it to full field was followed. The current was raised in 500 A steps starting from 3000 A and several spot heater quenches were induced at each new current. Strip heaters were fired promptly when the quench was detected while the dump trigger was progressively delayed until the magnet absorbed all its own energy. (The power supply was phased back promptly in all cases.) Limits were placed on various quantities to insure the safety of the magnet (see Table 3); the procedure was to be modified if it appeared that any limit would be exceeded at the next current.

This program was carried out at currents of 3000 A and 3500 A. Higher current operation was not possible because the superconducting part of the positive power lead was found to quench at 3630 A. The magnet and feed can have been warmed to room temperature to allow repair of the power lead and we expect to bring the magnet to full field in the near future. Table 4 summarizes the 3000 A and 3500 A quenches.

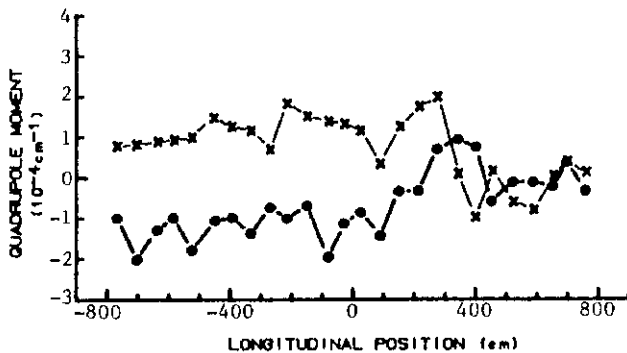


Figure 6. Normal (x) and skew (.) quadrupole moments as a function of position along the magnet. The origin is at the magnet center and positive positions are towards the lead end.

Table 3

Safety limits for SSC prototype magnet testing

MIITs	11 $10^6(A)^2\text{sec}$
Total Voltage	2000 V
Resistive Voltage	3000 V
Interconnect Pressure	150 psia
Magnet Center Pressure	250 psia
End-to-end Pressure Difference	50 psi
Force on Center Anchor	6000 lb

Table 4

Summary of Quench Data

	3000	3500 A
Current	3000	3500 A
Detection Time	0.16	0.12 sec
MIITs	6.9	7.8 $10^6(A)^2\text{sec}$
V_{max}	-32	-35 V
(IR) _{max}	214	335 V
R_{max}	165	225 m Ω

Figures 7-12 summarize data taken from two 3500 A quenches induced with a spot heater near the return end. Fig. 7 shows the magnet current and coil resistance as a function of time. (In all plots of quench data in this paper $t=0$ is defined to be the time at which the quench was detected. The delay

between the triggering of the spot heater and the detection of the quench is the "detection time" quoted in Table 4.) The temperature of the helium emerging from the coil, as measured inside the dogbone ends, is plotted in Fig. 8, while the pressure in the interconnect regions is displayed in Fig. 9. The pressure initially falls because the relief valves are opened when the quench is detected. As energy is transferred to the helium, the pressure rises rapidly and then falls. The slow rise for times later than five seconds corresponds to the rise in pressure in the external manifold into which the helium is directed. Because the line from the relief valve to the interconnect region is shorter at the return than at the feed end, a difference in pressure between the two ends of about 10 psi exists for about 100 msec, exerting a momentary force of approximately 1000 pounds on the cold mass. The strain on the two axial anchors during the first second is displayed in Fig. 10, showing that the cold mass oscillates longitudinally as a result of this impulse.

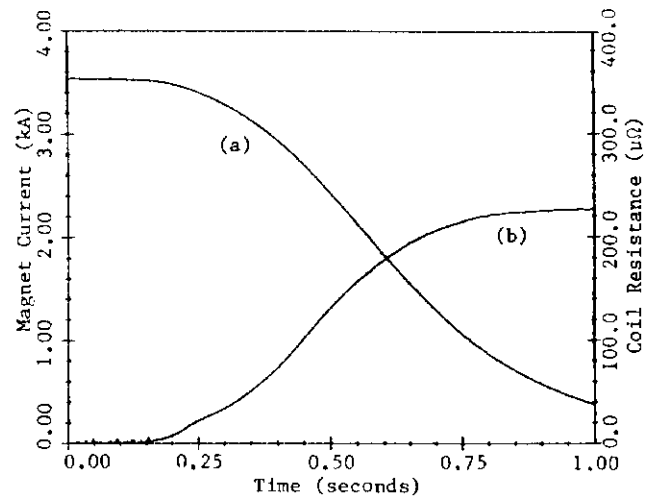


Figure 7. Magnet current (a) and coil resistance (b) as a function of time. The quench was induced at $t = -0.12$ sec with a spot heater mounted on the parting plane between the upper and lower inner coils. Two strip heaters were triggered when the quench was detected ($t=0$).

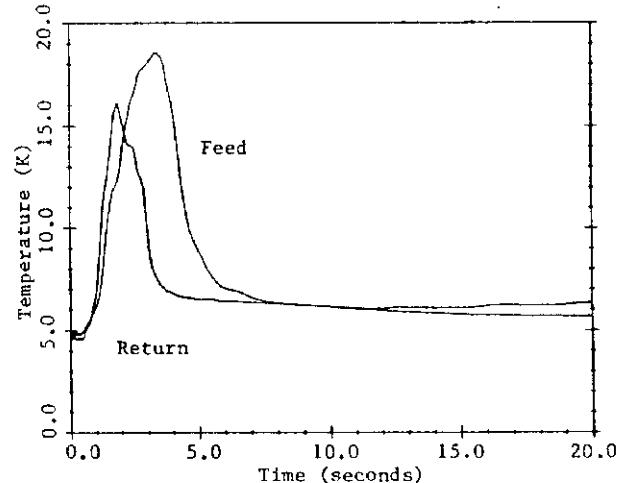


Figure 8. Temperature of helium exiting the annular region between the coil and the beam pipe as a function of time after the quench is detected. Temperature is measured by 100 Ω , 1/8 watt carbon resistors mounted inside the dogbone ends of the magnet.

The behavior of the magnet in the quenches discussed above is dominated by the firing of the strip heaters. To allow the study of "natural" quench propagation at 3500 A, one quench was induced in which the strip heater trigger was delayed by 200 msec after the quench was detected. The spot heater used to initiate this quench is located on the parting plane between the lower and upper inner coils and is in closer contact with the lower coil. Thus we expect the quench to develop last in the upper outer quarter coil. Fig. 11 shows the difference in voltage between the two outer coil quarters. No voltage difference develops until 160 msec after the quench is detected when the lower coil begins to go normal. We are thus able to use the upper outer quarter coil to measure dI/dt in order to extract the resistive components of the voltages in the inner coils. (This gives a less "noisy" measure of dI/dt than does the dI/dt coil.)

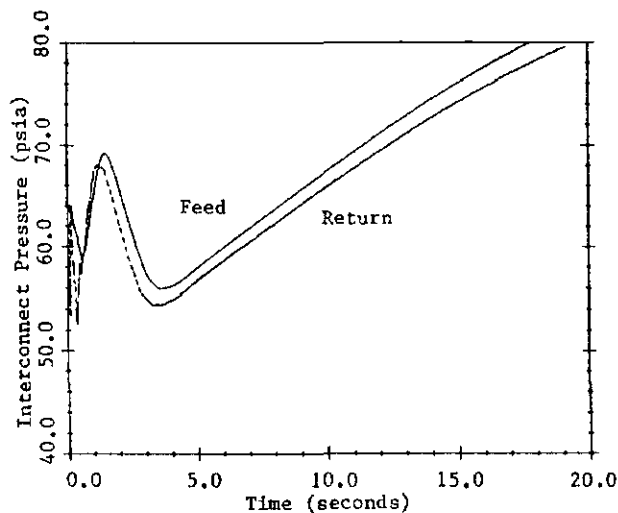


Figure 9. Pressure in the interconnect regions as a function of time after the quench is detected.

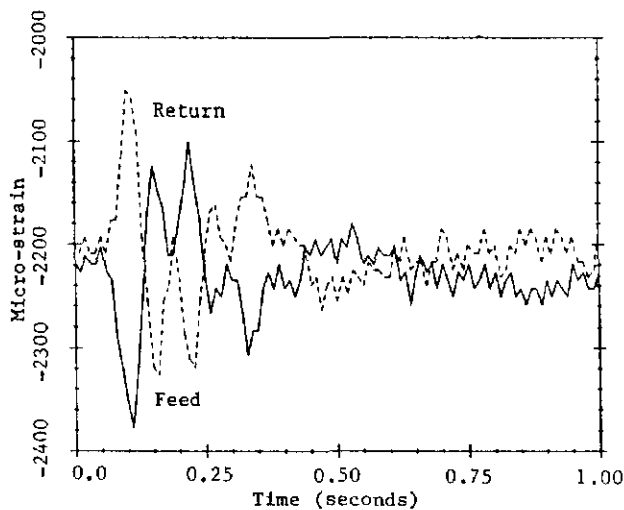


Figure 10. Strain on the axial restrain anchors as a function of time after the quench is detected. One micro-strain corresponds to a force of approximately one pound¹³ on an individual anchor.

The resistances of the lower inner and upper inner coils as a function of time are plotted in Fig. 12. (The "glitch" at 160 msec occurs when the power supply shuts off. As the magnet current is

discharged through the approximately 10 m Ω of electrical bus between the power supply and the magnet, the large dI/dt sets up eddy currents in the iron yoke that alter the ratio of inner coil to outer coil inductance.) Discontinuities in the slopes of the two curves are apparent at the points marked by arrows. These slope changes occur when the quench propagates from one winding to the next, increasing the number of cables in which resistance is growing. The time between discontinuities measures the transverse quench velocity while the slope, divided by the number of quenching turns, yields the longitudinal velocity. The curve for the lower coil can be followed until five turns have quenched. The data are summarized in Table 5 and Fig. 13. The longitudinal and transverse velocities measured here are similar to those measured in a test apparatus at Fermilab which simulates a small length of a magnet²¹ and in a 4.5 m model magnet at Brookhaven.²²

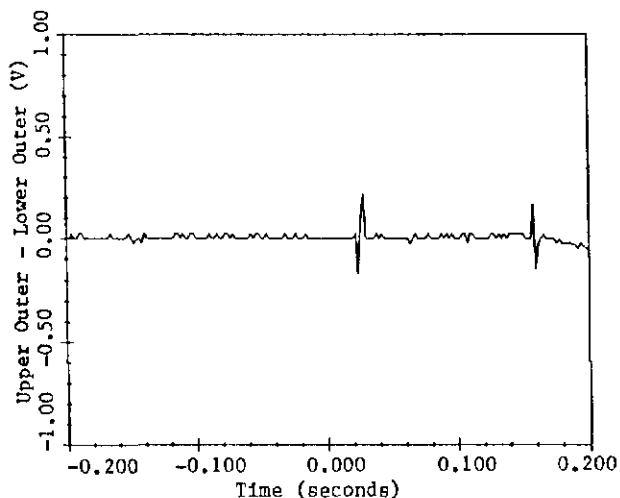


Figure 11. Voltage across the upper outer quarter coil minus the voltage across the lower outer quarter coil as a function of time after the quench is detected. The quench was induced at a current of 3500 A with a spot heater on the parting plane between the upper and lower inner quarter coils. Two strip heaters were triggered 0.2 seconds after the quench was detected.

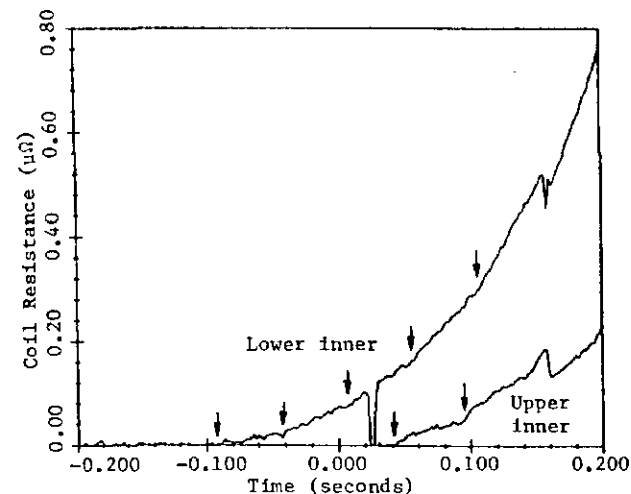


Figure 12. Resistances of the lower inner quarter coil and the upper inner quarter coil as a function of time after the quench is detected. The quench was induced at a current of 3500 A with a spot heater on the parting plane between the upper and lower inner quarter coils. Two strip heaters are triggered 0.2 seconds after the quench is detected.

Table 5

Longitudinal and transverse quench velocity data. The longitudinal velocity in meters/second has been computed using the measured²¹ resistance of the inner coil cable of $36 \pm 1.5 \mu\Omega/\text{meter}$ and corresponds to the velocity of one end of the normal zone.

Lower Inner Coil

#Turns	Slope	Δt	Longitudinal Velocity
1	0.4 m Ω /sec	50 msec	5.6 m/sec
2	1.0 m Ω /sec	50 msec	6.7 m/sec
3	1.9 m Ω /sec	48 msec	8.8 m/sec
4	2.8 m Ω /sec	46 msec	9.8 m/sec
5	4.4 m Ω /sec	--	12.3 m/sec

Upper Inner Coil

#Turns	Slope	Δt	Longitudinal Velocity
1	0.7 m Ω /sec	50 msec	9.8 m/sec
2	1.6 m Ω /sec	50 msec	11.2 m/sec

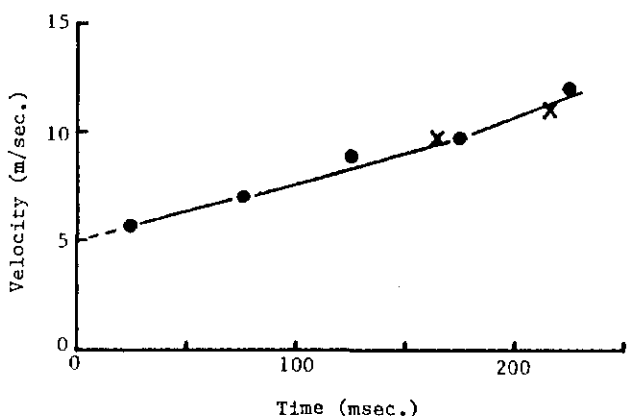


Figure 13. Longitudinal quench propagation velocity at 3500 A as a function of time after the quench is induced. Velocity corresponds to the propagation of a single normal zone front. Data from the lower coil are plotted as "•" while those from the upper coil are plotted as "x."

Acknowledgements

We enthusiastically acknowledge the dedicated efforts of the members of the technical staff of the Fermilab Magnet Development and Test Facility without whose assistance the tests reported here would not have been possible. We thank in particular R. Barger, A. Bianchi, J. Garvey, D. Harness, S. Helis, C. Hess, C. Ioriatti, F. Johnson, G. Kirschbaum, D. Krause, D. Lewis, K. McGuire, W. Mumper, R. Nehring, J. Pachnik, A. Rusy, E. Schmidt, H. Stahl, J. Tague, D. Validis, R. Voigts, H. Warren, D. Wendt, F. Wilson, and W. Zimmerman.

References

1. P. Dahl, et al., "Construction of Cold Mass Assembly for Full Length Dipoles for the SSC

- Accelerator," Proc. of the Applied Superconductivity Conference, Baltimore, MD (1986), J. Schooley (Ed.).
2. "Conceptual Design of the Superconducting Super Collider," SSC Central Design Group, Lawrence Berkeley Laboratory, One Cyclotron Road, Berkeley, CA 94720.
3. R. C. Niemann, et al., "Design, Construction and Test of a Full Scale SSC Dipole Magnet Cryostat Thermal Model," Proc. of the Applied Superconductivity Conference, Baltimore, MD (1986), J. Schooley (Ed.).
4. R. Barger, et al., "Operating History of Fermilab's 1500 W Refrigerator Used for Energy Saver Magnet Production and Testing," *Advances in Cryogenic Engineering* 31 (1986).
5. Model CGR-1-1000, LakeShore Cryotronics, Inc., Westerville, Ohio.
6. Model N2K, Scientific Instruments, Inc., Lake Worth, Florida.
7. Later magnets will have "straight" ends.
8. Model 831, Dynisco, Norwood, Massachusetts.
9. Model 603B1, Kistler Instrument Corporation, Amherst, New York.
10. Model 705, Keithley Instruments, Inc., Cleveland, Ohio.
11. Model 3457, Hewlett Packard Co., Palo Alto, California.
12. Model 8212A, LeCroy Research Systems Corporation, Spring Valley, New York.
13. Model F100000-100, Empro Manufacturing Co., Inc., Indianapolis, Indiana.
14. A higher threshold was required for the magnet voltage minus the appropriately weighted signal from the dI/dt coil than from the magnet alone because of substantial capacitive pickup in the dI/dt coil. This will be eliminated in later tests by modifying the dI/dt coil geometry.
15. Approximately 40% of the axial strength comes from the anchors; the remainder comes from the five posts and from the bellows at the ends of the cold mass.
16. M. Kuchnir, et al., "NMR Measurements in SSC Dipole D00001," TM-1240 (1986), Fermi National Accelerator Laboratory, Batavia, Illinois.
17. P. Wanderer, "Production Techniques for Measuring SSC Accelerator Magnets," Proc. of the ICFA Workshop on Superconducting Magnets and Cryogenics, Brookhaven National Laboratory (1986), P. Dahl (Ed.).
18. K. Borer and G. Fremont, "The Nuclear Magnetic Resonance Magnetometer, Type 9298," CERN 77-19.
19. Model 9836, Hewlett Packard Co., Palo Alto, California.
20. A. W. Chao, "Magnet Field Quality Requirements for the SSC," Proc. of the ICFA Workshop on Superconducting Magnets and Cryogenics, Brookhaven National Laboratory (1986), P. Dahl (Ed.).
21. M. Kuchnir, et al., "Transversal Quench Propagation Measurement," Proc. of the Applied Superconductivity Conference, Baltimore, MD (1986), J. Schooley (Ed.).
22. G. Ganetis and A. Prodell, "Results from Heater-Induced Quenches of a 4.5 m Reference Design D Dipole for the SSC," Proc. of the Applied Superconductivity Conference, Baltimore, MD (1986), J. Schooley (Ed.).